

Research Article

Detection of Underground Utility Pole Base for Distribution Transmission Network Based on Transient Electromagnetic Method

Jun Zhou^{1,*} , Tianyi Tao¹ , Lingda Xu² , Yonglin Zhi² 

¹High Magnetic Group, Songshan Lake Mat Lab, Dongguan, China

²Baisha Power Supply Bureau, Hainan Power Grid Corporation, Haikou, China

Abstract

In the construction of overhead distribution network lines, ensuring the stability and construction quality of utility pole foundations is crucial. Traditionally, this process may involve excavation and direct inspection, which is not only time-consuming but may also cause environmental damage. The non-destructive detection scheme proposed in this paper, based on the transient electromagnetic method (TEM), offers an efficient and non-intrusive method for detecting the burial conditions of utility pole bases, pulls, and chucks. The transient electromagnetic method is a geophysical exploration technique that uses the principle of electromagnetic induction to detect the distribution of underground materials. When detecting utility pole bases, this method analyzes the electromagnetic response generated by underground metallic structures to obtain information. However, traditional TEM has a blind zone problem in shallow metal detection, which limits its application in utility pole base inspection. To address this issue, the scheme proposed in this paper introduces a decoupling coil to eliminate interference caused by the primary magnetic field. This decoupling technology significantly improves the detection discrimination, allowing for a more accurate determination of the burial depth and condition of bases, pulls, and chucks. Finite element numerical analysis using COMSOL 5.4 is adopted to examine the underground magnetic field distribution and optimize coil parameters. This analysis helps to understand the interaction between the electromagnetic field and underground structures, guiding the design of coils and the development of detection strategies. The prototype experimental platform built further validates the effectiveness of the scheme. Experimental results include measured data of magnetic field variations, assessments of detection depth and resolution. These experimental results are crucial for verifying the practical application potential of the non-destructive detection scheme.

Keywords

Transient Electromagnetic (TEM) Method, Decoupling, Mental Detection, Non-Destructive Testing, Utility Pole, Base

1. Introduction

To prevent the utility poles of transmission and distribution lines from being pulled up, sinking and lodging, the base,

pull and chuck (BPC) are often used for reinforcement. [1] In practical application, to check whether the depth of under-

*Corresponding author: 15827204180@163.com (Jun Zhou)

Received: 16 June 2024; **Accepted:** 2 July 2024; **Published:** 15 July 2024



Copyright: © The Author(s), 2024. Published by Science Publishing Group. This is an **Open Access** article, distributed under the terms of the Creative Commons Attribution 4.0 License (<http://creativecommons.org/licenses/by/4.0/>), which permits unrestricted use, distribution and reproduction in any medium, provided the original work is properly cited.

ground base reaches the standard, manual soil excavation is often used for sampling inspection of the BPC. However, manual excavation is time-consuming, laborious, and inefficient, and the facility may be damaged during trenching process. Therefore, it is necessary to use non-excavation technology to detect whether the installation depth of underground BPC meets the standard. Generally, BPC are made of steel mesh and concrete, thus the detection can be achieved by inspecting internal steel structure. [2]

Transient Electromagnetic Method (TEM) is a time domain electromagnetic exploration method, [3, 4] which is widely used in mineral exploration, geothermal and crustal structure investigation, geophysical and engineering exploration. [5, 6] TEM detection is also one of the most important methods of metal detection. [7] Thus, this paper intends to apply TEM to detect BPC. Conventional TEM detection system mainly comprises transmitting and receiving coils. [8] The pulse current is employed as excitation source. [9] While current in transmitting coil is suddenly turned off, high di/dt generates a high magnetic field which is denoted as “primary field”. [10] Induced current, known as eddy current or secondary current, is formed when primary magnetic field encounter underground ferromagnetic substance. Such time-varying secondary current also generates new magnetic field which is denoted as “secondary field”. [11] Eigenvalues extracted from the secondary field can be applied to determine the characteristics and location of targeted objects. [12] However, owing to the inductive transmitting coil, current in the transmitting coil does not abruptly go to zero after the switch is turned off. [13] Residual primary field generated by that transient current will induce disturbing voltage on the receiving voltage at the very early time, which makes it difficult to acquire the pure signal induced by secondary field. Confined by the transient process of transmitting coil mentioned above, early receiving signal of conventional TEM detection is ignored, which forms a detection blind zone within 0~20 meters. [14, 15] The depth of underground BPC is generally in the depth interval 0~3 meters, which just falls in this detection blind zone. And as a result, the interference from the primary field is inevitable. [16, 17] What's more, compared to BPC, metal structures inside the utility pole and pull wire are larger and closer to the detection device, which generates larger interference signals. [18] It is crucial to suppress the interference mentioned above. [19]

Based on the principle of space magnetic field cancellation, [20] a decoupling coil is introduced to offset induced voltage generated by primary field and utility pole. After extracting decoupled receiving voltage, the depth of detection objects can be accurately obtained, which reaches the requirement of the non-destructive examination for underground BPC of the utility pole.

2. Item Detection System

2.1. Detection Objects

Figure 1 illustrates the overall diagram of the detection system, which is mainly composed of the detection object, coil system, data acquisition system and pulse current source circuit. Detection object contains utility pole, base, pull, chuck and pull wire. The coil system mainly includes transmitting, receiving and decoupling coils. Considering the signal characteristics and detection requirements, air-core coils are adopted. Data acquisition system collects and processes the weak differential voltage of receiving and decoupling coils. There are many types of BPC affiliated to different utility poles. In this paper, the utility pole, D-40-09, with its supporting BPC is selected as the research target, and corresponding parameters are shown in Table 1.

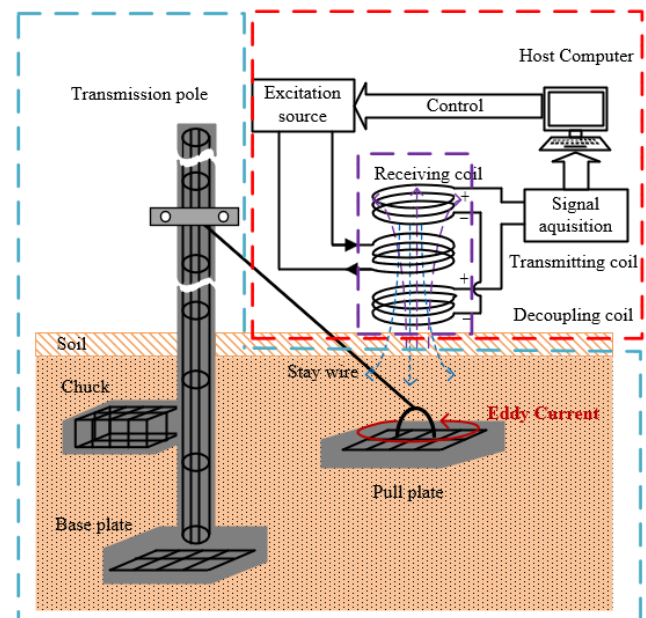


Figure 1. Schematic of detection object and system.

Table 1. Parameters of detection objects.

	Size (m)	Depth (m)
Utility pole	15.00	3.00
Base	0.60×0.53×0.15	3.00
Pull	0.95×0.50×0.28	1.25
Chuck	0.80×0.30×0.25	1.50

2.2. Principle of TEM Detection

To clarify the correlation between detection coils and targeted objects, metal conductor in detection objects is simpli-

fied as a coil, and eddy current generated in the conductor is equivalent to the current in the equivalent coil. After reasonable simplification, equivalent mutual inductance model of the detection system in Figure 2 can be obtained. Figure 2(a) and (b) are the conventional and proposed TEM equivalent model respectively. In Figure 2, coil 1 and 2 are the transmitting and receiving coil respectively; coil 3 and 4 are equivalent coils of the targeted object and utility pole respectively; coil 5 is the decoupling coil. $i_k, u_k, (k=1\sim 4)$ are the current and voltage in coil i of conventional TEM detection model. $i'_k, u'_k, (k=1\sim 5)$ are the current and voltage in coil i of proposed TEM detection model. h is the distance between transmitting and receiving coil. H is the distance between transmitting coil and targeted object.

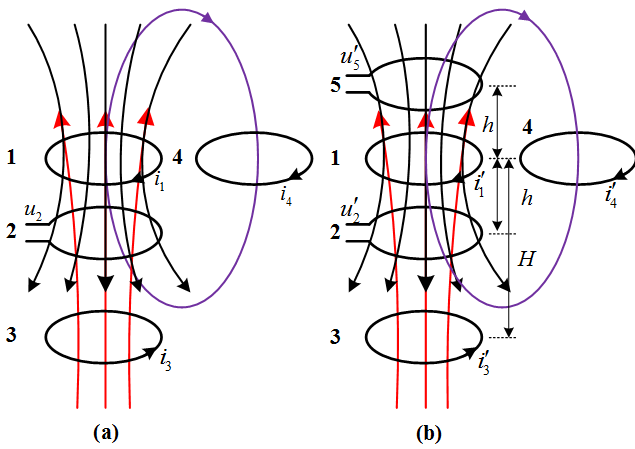


Figure 2. (a) the conventional TEM equivalent model. (b) TEM equivalent model with a decoupling coil.

According to the mutual inductance model in Figure 2(a), after ignoring coil resistance, the current and voltage in the conventional TEM detection equivalent model satisfy the following equation [21].

$$\begin{bmatrix} u_1(t) \\ u_2(t) \\ u_3(t) \\ u_4(t) \end{bmatrix} = \begin{bmatrix} L_{11} & M_{21} & M_{31} & M_{41} \\ M_{12} & L_{22} & M_{32} & M_{42} \\ M_{13} & M_{23} & L_{33} & M_{43} \\ M_{14} & M_{24} & M_{34} & L_{44} \end{bmatrix} \times \frac{d}{dt} \begin{bmatrix} i_1 \\ i_2 \\ i_3 \\ i_4 \end{bmatrix} \quad (1)$$

where M_{ij} ($i, j=1\sim 4; i \neq j$) is the mutual inductance between coil i and j , and L_{ii} ($i=1\sim 4$) is the self-inductance of coil i . Generally, receiving coil is usually highly resistive and approximately considered as open circuit, which means $i_2 \approx 0$. The Receiving voltage $u_{rec}(t)$ can be written as

$$u_{rec}(t) = u_2(t) = M_{12} \frac{di_1}{dt} + M_{32} \frac{di_3}{dt} + M_{42} \frac{di_4}{dt} \quad (2)$$

According to Faraday's law of electromagnetic induction, [9] eddy currents induced by ferromagnetic materials within

the detection object and utility pole are respectively expressed as

$$i_3(t) = \frac{M_{13}}{L_{33}} \frac{di_1}{dt} e^{-\frac{t}{\tau_3}} + \frac{M_{43}}{L_{33}} \frac{di_4}{dt} e^{-\frac{t}{\tau_3}} \quad (3)$$

$$i_4(t) = \frac{M_{14}}{L_{44}} \frac{di_1}{dt} e^{-\frac{t}{\tau_4}} + \frac{M_{34}}{L_{44}} \frac{di_3}{dt} e^{-\frac{t}{\tau_4}} \quad (4)$$

τ_3, τ_4 are time constants, which are determined by equivalent inductance and resistance of the two coils. [22] Since mutual inductance between the two equivalent coils (3 and 4) and eddy current in the coils is relatively small, the second term in (3) and (4) can be ignored. After bringing simplified (3) and (4) into (2), receiving voltage can be expressed as

$$u_{rec}(t) = u_{rec,1}(t) + u_{rec,2}(t) + u_{rec,3}(t) \quad (5)$$

where $u_{rec,1}(t) = M_{12} \frac{di_1}{dt}$, $u_{rec,2}(t) = \frac{M_{13}M_{32}}{L_{33}} \left[\frac{d^2 i_1}{dt^2} - \frac{1}{\tau_3} \frac{di_1}{dt} \right] e^{-t/\tau_3}$,
 $u_{rec,3}(t) = \frac{M_{14}M_{42}}{L_{44}} \left[\frac{d^2 i_1}{dt^2} - \frac{1}{\tau_4} \frac{di_1}{dt} \right] e^{-t/\tau_4}$.

$u_{rec,1}(t)$ is the primary field induced voltage; $u_{rec,2}(t)$ is the effective receiving voltage induced by eddy current in detection object; $u_{rec,3}(t)$ is the induced voltage produced by eddy current in utility pole and pull wire. Magnetic fields from coil 3 and 4 are generated by eddy current, and eddy current $i_{3,4}$ are much smaller than conducting current in transmitting coil. Thus the receiving voltage satisfies: $u_{rec,1}(t) \gg u_{rec,2}(t)$, $u_{rec,1}(t) \gg u_{rec,3}(t)$, which shows that the receiving voltage $u_{rec}(t)$ is mainly determined by $u_{rec,1}(t)$. Meanwhile, the volume of utility pole is much larger than that of the detection object, so the mutual inductance in equation (5) satisfies: $M_{14} \gg M_{13}$, $M_{24} \gg M_{23}$ and secondary field induced voltage meets $u_{rec,3}(t) > u_{rec,2}(t)$. The proportion of effective receiving voltage $u_{rec,2}(t)$ in the summation of the receiving voltage $u_{rec}(t)$ is very small. It is difficult to extract the tiny change of $u_{rec,2}(t)$ caused by distance change of detection object from the receiving voltage $u_{rec}(t)$. [23]

To effectively distinguish $u_{rec,2}(t)$ from $u_{rec}(t)$, $u_{rec,1}(t)$ and $u_{rec,3}(t)$ must be reduced. Therefore, a decoupling coil is introduced to reduce their interference. Decoupling TEM coil can be arranged in various ways. [24] Considering that the induced voltage generated by transmitting coil and utility pole should be simultaneously decoupled, receiving and decoupling coils are symmetrically placed with respect to transmitting coil, which is shown in Figure 2 (b). The parameters of the decoupling and receiving coils should be the same.

$$\begin{bmatrix} u'_1(t) \\ u'_2(t) \\ u'_3(t) \\ u'_4(t) \\ u'_5(t) \end{bmatrix} = \begin{bmatrix} L'_{11} & M'_{21} & M'_{31} & M'_{41} & M'_{51} \\ M'_{12} & L'_{22} & M'_{32} & M'_{42} & M'_{52} \\ M'_{13} & M'_{23} & L'_{33} & M'_{43} & M'_{53} \\ M'_{14} & M'_{24} & M'_{34} & L'_{44} & M'_{54} \\ M'_{15} & M'_{25} & M'_{35} & M'_{45} & L'_{55} \end{bmatrix} \times \frac{d}{dt} \begin{bmatrix} i'_1 \\ i'_2 \\ i'_3 \\ i'_4 \\ i'_5 \end{bmatrix} \quad (6)$$

According to TEM equivalent model in Figure 2 (b), (6) is obtained. M'_{ij} ($i, j = 1 \sim 5$; $i \neq j$) is the mutual inductance between coil i and j , and L'_{ii} is the self-inductance of coil i . Since decoupling and receiving coils are highly symmetrical, there is $M'_{12} = M'_{15}$. Currents in receiving and decoupling coils are approximately 0, and effective receiving voltage is the differential voltage of $u'_2(t)$ and $u'_5(t)$. Effective receiving voltage $u'_{rec}(t)$ can be presented as

$$u'_{rec}(t) = u'_2(t) - u'_5(t) = (M'_{23} - M'_{35}) \frac{di'_3}{dt} + (M'_{24} - M'_{45}) \frac{di'_4}{dt} \quad (7)$$

The receiving voltage $u'_{rec}(t)$ does not contain primary field induced voltage, so the interference from the primary field is fully eliminated. In addition, utility pole is long straight distribution and perpendicular to transmitting coil, so magnetic line generated by equivalent coil 5 is evenly and simultaneously cross-link decoupling and receiving coils, and magnetic field distribution is approximately symmetrical, which can cancel interference introduced by utility pole. This process suppresses the interference from utility pole. Although the effective receiving voltage is partially weakened, there is no primary field induced voltage in receiving voltage, and the secondary field induced voltage produced by utility pole has been well suppressed. The effective voltage is comparable with the incomplete decoupling voltage; hence small change of the targeted object position can be reflected in the receiving voltage. Adding a decoupling coil can improve the accuracy of the effective receiving voltage. [25]

As the utility pole is approximately symmetrical with respect to receiving and decoupling coils, $M'_{24} \approx M'_{25}$ is easily deduced, and (7) can be further simplified to (8).

$$u'_{rec}(t) = (M'_{23} - M'_{35}) \frac{di'_3}{dt} \quad (8)$$

The time-varying secondary field generated by eddy current in equivalent coil 3 induces voltage $\varepsilon_2(t)$ and $\varepsilon_5(t)$ in receiving and decoupling coils. After combining simplified (3), the effective receiving voltage $u'_{rec}(t)$ can be presented as

$$u'_{rec}(t) = \varepsilon_2(t) - \varepsilon_5(t) \approx \frac{M'_{13}(M'_{32} - M'_{35})}{L'_{33}} \left[\frac{d^2 i'_1}{dt^2} - \frac{1}{\tau_3} \frac{di'_1}{dt} \right] e^{-t/\tau_3} \quad (9)$$

$$= a_1 \cdot a_2 \cdot a_3$$

where $a_1 = \frac{d^2 i'_1}{dt^2} - \frac{1}{\tau_3} \frac{di'_1}{dt}$, $a_2 = M'_{13}(M'_{32} - M'_{35})/L'_{33}$, $a_3 = e^{-t/\tau_3}$.

Effects of exciting source on receiving voltage $u'_{rec}(t)$ can be presented in a_1 . Since the shape and material of detection objects are all standardized, intrinsic attributes of detection object, noted as a_3 , are all identical. The only component related to the depth of detection objects is a_2 . After determining the parameters of excitation source, detection objects and coils are all selected, the effective receiving voltage is mainly determined by mutual inductance between coil 1, 2, 4 and their parameters. Under specific detection depth, mutual inductance is affected by the distance h between receiving, decoupling and transmitting coils. As shown in Figure 2(b), in principle, larger distance between the coils results in higher differential voltage. However, confined by coil placement, an increase in h will finally increase H , which leads to the decrease of actual a_2 . There is a theoretical optimum h whose specific value is related to the coil parameters, which will be discussed in Sector III. After determining h , a_2 is mainly determined by the distance between detection object and transmitting coil H . The receiving voltage can be used to deduce the depth of the detecting object.

2.3. Design of the Pulse Excitation Source Circuit

The pulse current source circuit shown in Figure 3 is designed considering safety and portability. [26] This circuit consists of a transmitting coil, a 1700 V IGBT, a DC power supply and auxiliary buffer elements. R_L and L are equivalent resistance and inductance of transmitting coil; power supply V_e is a 24 V lithium battery; R_0 is used for current limiting; RC are in parallel with IGBT. di/dt of the circuit is larger at the falling edge than at the rising edge, so falling edge is used as the effective period in detection. In this design, 50ms/5s signal is applied as the IGBT trigger.

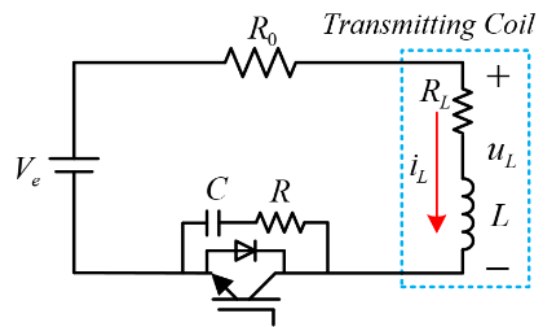


Figure 3. Schematic of the pulse current source circuit.

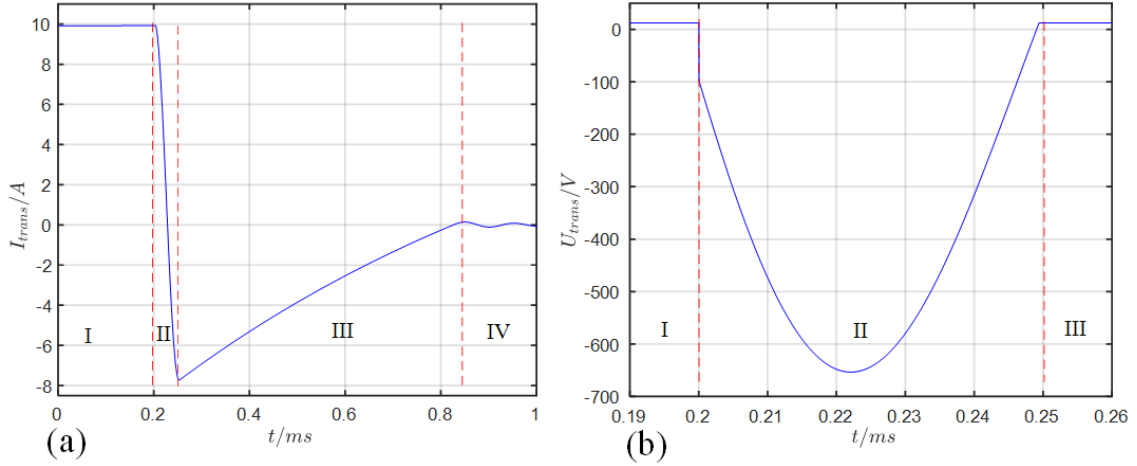


Figure 4. (a) Current waveform at falling edge. (b) Voltage waveform during stage II.

Voltage and current waveforms of the pulse current source at falling edge are shown in Figure 4. In stage I, the pulse current reaches a steady state. The current in the loop does not change at the beginning of stage II, but smoothly changes from stage I to II. During this transition, IGBT converts from conducting state to off state, causing a sudden change in transmitting voltage across the coil in Figure 4(b). During stage II, IGBT has been completely turned off, and a second-order RLC series circuit is formed when the current flows through RC snubber circuit, and the peak voltage is generated at current zero-crossing point. In stage III, the pulse current flows through the body diode, and RL circuit is generated for RC snubber circuit is bypassed. The coil current slowly changes from negative to positive. After stage III, the body diode cuts off, and RLC oscillation circuit is formed again. Oscillation exponential attenuation waveform forms in the voltage and current of the transmitting coil during stage IV.

2.4. Oscillation Suppression of Receiving Coil

It should be noted that sudden change of the transmitting current introduced by IGBT turn-off at the beginning of stage II in Figure 4 will finally be applied to receiving coil through electromagnetic induction, which may result in high-frequency oscillation in receiving coil. The equivalent circuit diagram of receiving coil is shown in Figure 5. e is the coil induced voltage. r , L and C_r are receiving coil resistance, inductance and distribution capacitance respectively, which are related to the coil winding form, the number of turns and geometric parameters. R_{in} and C_{in} are input resistance and capacitance of amplifier. R_D is the damping resistor. To simplify analysis, $C = C_r + C_{in}$ and $R = R_{in} // R_D$ are defined. In general, $R_{in} \gg R_D$, so $R = R_{in} // R_D \approx R_D$. The 2-order equivalent circuit of receiving coil can be expressed as

$$e(t) = LC \frac{d^2 u_m(t)}{dt^2} + \left(\frac{L}{R} + rC \right) \frac{du_m(t)}{dt} + \left(1 + \frac{r}{R} \right) u_m(t) \quad (10)$$

When $t \geq 0$, (10) is a homogeneous equation, and solution of this characteristic equation is

$$s_{1,2} = \frac{2\pi}{\tau_p} (-K \pm \sqrt{K^2 - 1}) \quad (11)$$

where $K = \sqrt{\alpha} \left(\frac{1}{2R} \sqrt{L/C} + \frac{r}{2} \sqrt{C/L} \right)$, $\alpha = \frac{R}{R+r}$, $\lambda = \frac{t}{\tau_p}$
 $\tau_p = 2\pi \sqrt{LC\alpha}$.

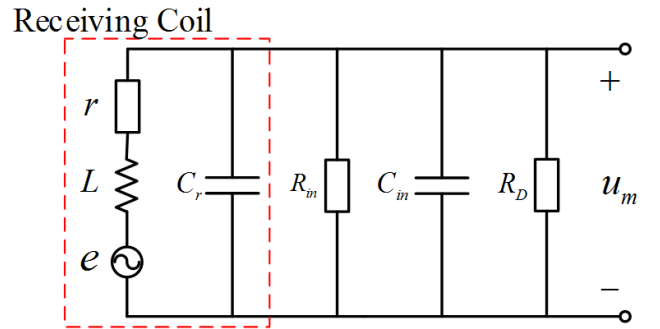


Figure 5. Equivalent circuit diagram of receiving coil.

According to (11), while $K < 1$, the step signal included in pulsed current cause oscillation in the receiving coil, which results in serious distortion of receiving voltage.

The step signal introduced by IGBT turn-off and free-wheeling diode cut-off in the transmitting coil is unavoidable. While working under over-damped or critical damped conditions, $K \geq 1$, oscillation is completely suppressed. However, overdamp ($K > 1$) may decrease output voltage u_m , which leads to lower signal-to-noise ratio (SNR). Damping resistor R_D should be selected to operate near critical damped conditions for oscillation suppress and smaller effective receiving voltage slash.

3. Simulation and Experiments

3.1. Simulation Study of PBC Detection

Theoretical analyses in Sector II show that effective receiving voltage is closely relative to coil parameters and their position. However, it is quite difficult to solve such model by analytical methods. In this paper, finite element simulation software COMSOL is used to determine coil parameters. A three-dimensional model with the pull as the detection object in Figure 6 is built in COMSOL 5.4, which is identical to Figure 1. Transmitting, receiving and decoupling coils are symmetrical. Coil diameter D is the mainly factor that affects receiving voltage. With the same detection depth, coil distance h and coil turn, the peak value of decoupled receiving voltage under varied coil diameter D is plotted in Figure 7.

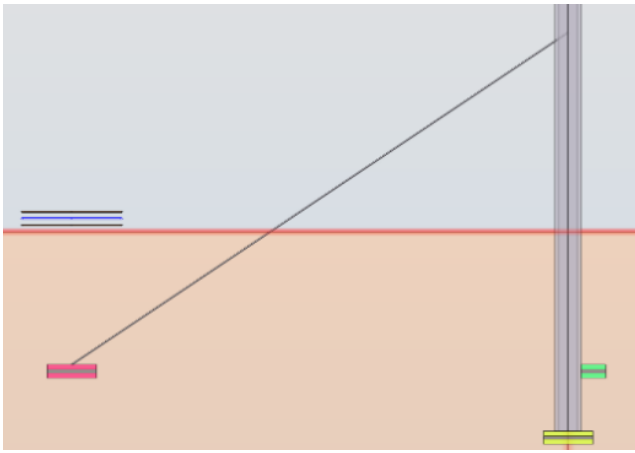


Figure 6. Three-dimensional simulation model in COMSOL.

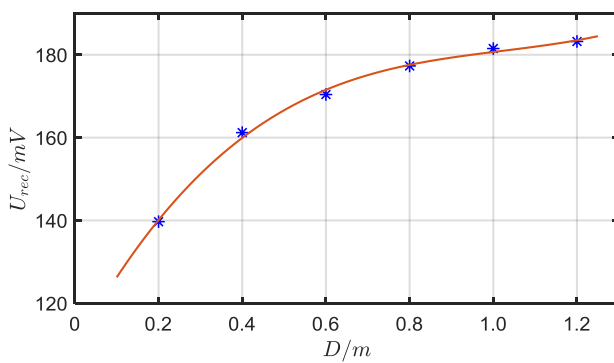


Figure 7. Correlation between coil diameter and peak receiving voltage.

Figure 7 shows that decoupled receiving voltage is promoted after increasing coil diameter. However, larger diameter is more vulnerable to ambient electromagnetic noise, which deteriorates detection resolution. Therefore, smaller diameter is advisable while ensuring the required detection depth. Simulation curves in Figure 8 show that peak value of

the receiving voltage slowly increases under $D > 0.6$ m, so coil diameter is set to 0.6 m to reach a compromise between larger receiving voltage and lower ambient electromagnetic noise. Coil turn n directly effects the amplitude of receiving voltage and transient characteristics, and the number of turns is preset as 30. According to long-term TEM simulation and experiments, the optimum value of coil distance h is close to $0.5D$. Simulation parameters are preset as follows: $D = 0.6$ m, $n = 30$, $h = 0.3$ m.

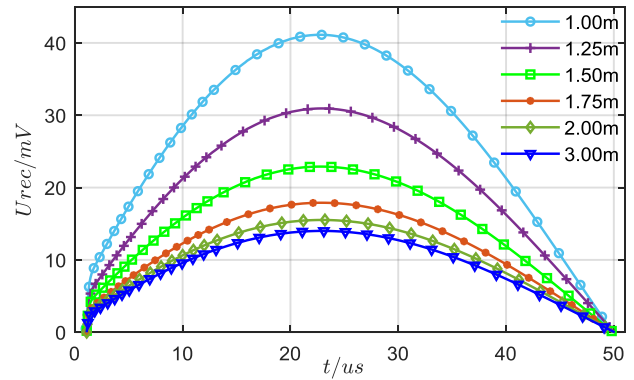


Figure 8. Receiving voltage waveform of simulation at falling edge.

After adjusting the buried depth of the pull, decoupled receiving voltage waveform shown in Figure 8 is obtained. The Waveform of receiving voltage is consistent with that of the transmitting coil. The change of the distance between pull and transmitting coil causes the peak voltage to change. The depth of the targeted object can be determined by detecting the induced differential voltage of the receiving and decoupling coils.

3.2. Experiment Result

The induced voltage produced by eddy current in receiving and decoupling coils is relatively small, therefore it is necessary to amplify the original signal and use amplified signal to deduce the depth of detecting object. In acquisition system, MODEL SR560 with maximum gain of 500,000 is used as low-noise preamplifier, which is capable of amplifying this weak induced voltage produced by eddy current. NI PXIe-5105 module with maximum sampling rate of 60 MHz is used as data acquisition card. In this experiment, the pre-amplifier is set as low-pass filter with 30 kHz cut-off frequency to suppress ambient electromagnetic noise. The Preamplifier gain is adjusted according to receiving voltage strength to acquire appropriate voltage range. Receiving and decoupling coils with a diameter 0.6 m are finally designed. Coils are wound with 0.40 mm enameled wire with 15 turns per layer and 30 turns in total. In winding process, number of turns in each layer is strictly controlled, and inductance, distributed capacitance and resistance of decoupling and receiving coils are strictly consistent. The Detection prototype

is shown in Figure 9. The Simulation shows that peak value of the receiving voltage corresponds to the fastest change of the current in transmitting coil. Therefore, peak voltage of receiving coil is selected as the eigenvalue in depth detection.

Affected by the interference from experimental equipment

and ambient electromagnetic noise, the receiving voltage contains white noise, impulse and burrs. Therefore, the average value of multiple measurements is adopted to further enhance SNR.

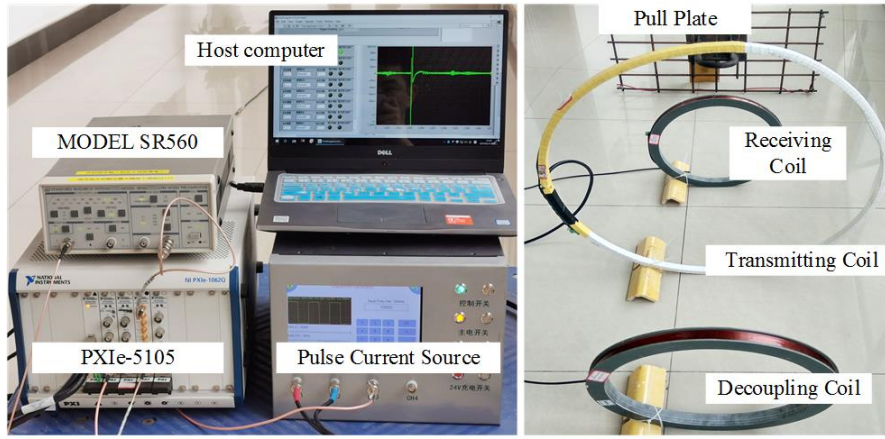


Figure 9. Prototype test platform for BPC Detection.

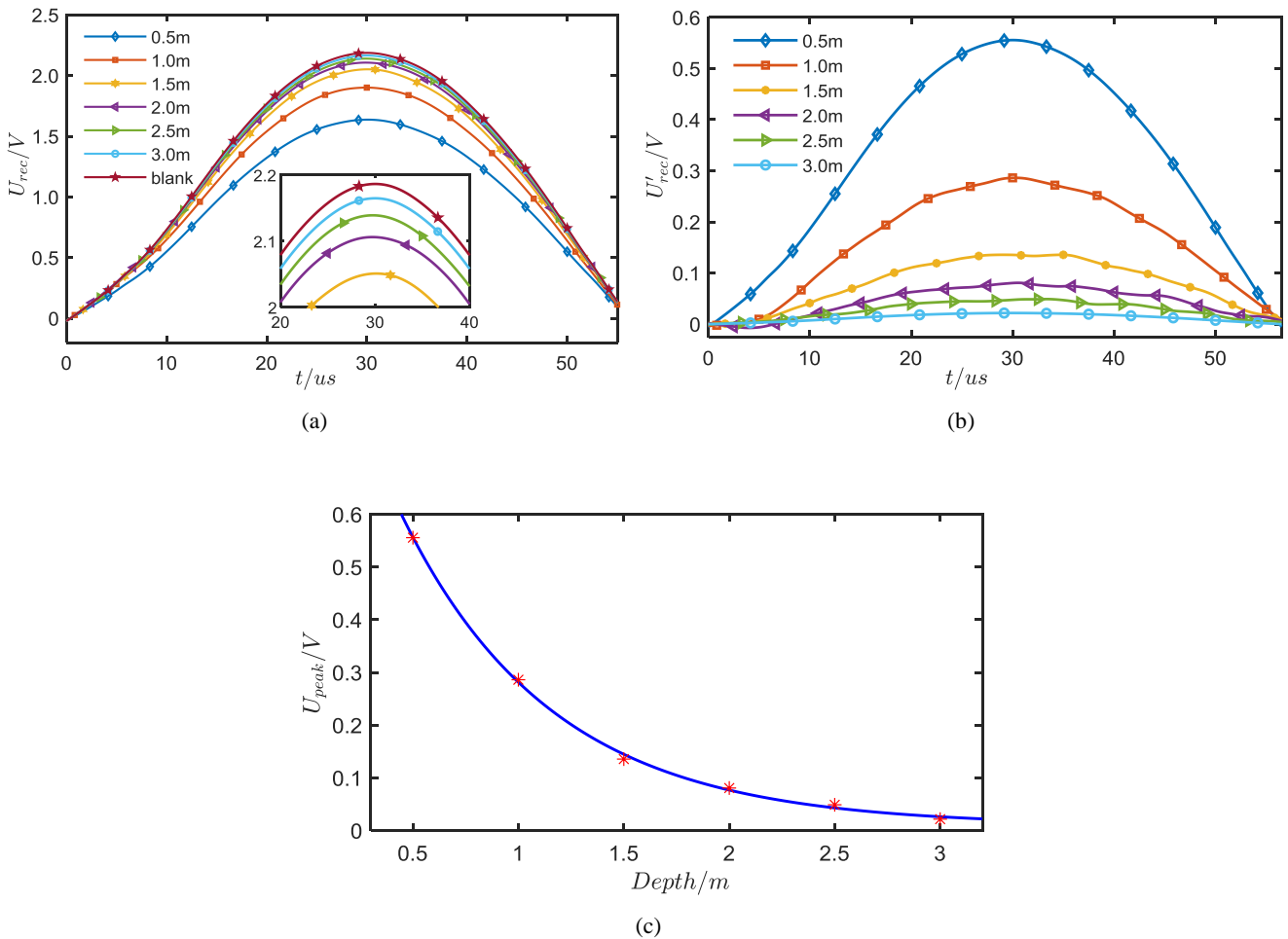


Figure 10. (a) Curves of receiving voltage with depth ranging from 0.5 m to 3.0 m. The curve, denoted “blank”, is obtained without detection objects. Due to ambient electromagnetic noise, receiving voltage curves are processed by taking 5 data sets for the mean filter in each depth scale. (b) Curves of the effective receiving voltage after subtracting the incomplete decoupling voltage. (c) Fitting curve of receiving voltage versus depth.

Owing to minor differences of coil parameters in production, there is still a small incomplete decoupling voltage in receiving voltage, which can be seen from curve “blank” in Figure 10(a). Incomplete decoupling voltage should be deducted from receiving voltage. After subtracting the incomplete receiving voltage from receiving voltage, the effective receiving voltage waveform is shown in Figure 10(a), which is consistent with the simulation waveform in Figure 8.

As BPC and utility pole are all standardized, the buried depth of target objects is reversely resolved through the effective receiving voltage. The correlation between receiving peak voltage and detection depth is obtained by experiment. This relation is approximately exponential, so curve fitting function $u(h) = ae^{bh} + c$ is introduced. Based on the received voltage in Figure 10(b), the relation is obtained as follows

$$u(h) = 1.103e^{-1.398H} + 0.009612 \quad (12)$$

The goodness of fit is $r^2 = 0.9991$, which shows that fitting effect is acceptable ($H \leq 3\text{m}$). Comparing experiment results with the simulation curve, owing to incomplete decouple, there is an offset voltage in experiment wave, but the trend of the voltage waveform of the receiving coil is identical. The depth of the targeted objects can be obtained by solving (12). Above methods can be extend to the detection of base and chuck.

4. Conclusions

This paper presents an innovative technique for detecting utility pole BPC using the TEM, while also introducing a decoupling coil to minimize interference caused by the primary field. The mathematical underpinnings of the proposed detection method are explained in depth, and the model's validity is confirmed through a comparison with the traditional TEM detection model. Optimization of coil parameters is achieved via finite element numerical analysis, and a prototype experimental platform is created. Simulation results and experimental data both confirm the proposed detection scheme's capability to precisely determine the depth of BPC.

In essence, this research introduces a non-destructive detection scheme that successfully overcomes the blind zone limitations of conventional TEM for shallow metal detection, thanks to a combination of sophisticated numerical simulation and rigorous experimental validation. This approach not only upgrades the quality and efficiency of overhead distribution network line construction but also reduces environmental harm, thereby fostering the sustainable growth of the power industry. With ongoing technological progress and refinement, this non-destructive detection scheme is expected to emerge as a standard tool for inspecting and maintaining power infrastructure.

Abbreviations

TEM	Transient Electromagnetic Method
BPC	Base, Pull and Chuck

Author Contributions

Jun Zhou: Conceptualization, Data curation, Formal Analysis, Funding acquisition, Investigation, Methodology, Project administration, Resources, Software, Supervision, Validation, Visualization, Writing – original draft, Writing – review & editing

Tianyi Tao: Data curation, Formal Analysis, Funding acquisition, Investigation, Resources, Validation, Visualization

Lingda Xu: Funding acquisition, Investigation, Project administration, Resources, Supervision, Validation

Yonglin Zhi: Funding acquisition, Investigation, Project administration, Resources, Supervision, Validation

Data Availability Statement

The data that support the findings of this study are available from the corresponding author upon reasonable request.

Conflicts of Interest

The author(s) declared no potential conflicts of interest with respect to the research, authorship, and/or publication of this article.

References

- [1] Wang CY, Liang XD, Emerson PA, et al. Investigation of Seasonal Variations of Tower Footing Impedance in Transmission Line Grounding Systems. *IEEE Transactions on Industry Applications* 2021; 57(3): 2274-2284. <https://doi.org/10.11648/j.ijmsa.20221103.12>
- [2] Alexandra I K, Bauyrzhan A U and Yurii V. T. Methodology for Analysing the Technical State and Residual Life of Overhead Transmission Lines. *IEEE Transactions on Power Delivery* 2021; 36(5): 2730-2739. <https://doi.org/10.1109/TPWRD.2020.3025929>
- [3] Smith RS, Annan AP, Lemieux J, et al. Application of a modified GEOTEM system to reconnaissance exploration for Kimberlites in the Point Lake area, NWT, Canada. *Geophysics* 1996; 61(1). 82-92. <https://doi.org/10.1190/1.1443959>
- [4] Tang RJ, Li FS, Shen FL, et al. Fast Forecasting of Water-Filled Bodies Position Using Transient Electromagnetic Method Based on Deep Learning. *IEEE Transactions on Geoscience and Remote Sensing* 2024; 62: 4502013. <https://doi.org/10.1109/TGRS.2024.3355543>

- [5] Chen J, Zhang Y and Lin TT. High-Resolution Quasi-Three-Dimensional Transient Electromagnetic Imaging Method for Urban Underground Space Detection. *IEEE Transactions on Industrial Informatics* 2023; 19(3): 3039-3046. <https://doi.org/10.1109/TII.2022.3176890>
- [6] Witherly K, Irvine R, and Godbout M. Reid Mahaffy test site, Ontario Canada: An example of benchmarking in airborne geophysics. In: *Proc. 74th Annu. Int. Meeting, Soc. Explor. Geophysicists, Denver, CO, USA, Oct, 2004*, pp. 1202–1204. <https://doi.org/10.1190/1.1843294>
- [7] Zhu X, Su X, Tai HM, et al. Bipolar steep pulse current source for highly inductive load. *IEEE Trans. Power Electron* 2016; 31(9): 6169–6175. <https://doi.org/10.1109/TPEL.2015.2503383>
- [8] Wang Q, Wang H, Wu M, et al. Research on Noise Suppression Method for Transient Electromagnetic Signal. In: *IEEE Advanced Information Management, Communicates, Electronic and Automation Control Conference (IMCEC)*, 2018, pp. 394-397. <https://doi.org/10.1109/IMCEC.2018.8469591>
- [9] Yu C, Fu Z, Wu G, et al. Configuration Detection of Substation Grounding Grid Using Transient Electromagnetic Method. *IEEE Transactions on Industrial Electronics* 2017, 64(8): 6475-6483. <https://doi.org/10.1109/TIE.2017.2682033>
- [10] Qin SQ, Wang Y, Xu Z, et al. Fast Resistivity Imaging of Transient Electromagnetic Using ANN. *IEEE Geoscience and Remote Sensing Letters* 2019; 16(9): 1373-1377. <https://doi.org/10.1109/LGRS.2019.2900992>
- [11] Gang Z, Rui X, Yu C, et al. Research on Double Coil Pulse Eddy Current Thickness Measurement. In: *2017 10th International Conference on Intelligent Computation Technology and Automation (ICICTA)*, 2017, pp. 406-409. <https://doi.org/10.1109/ICICTA.2017.97>
- [12] Shi X and Tao F. Research on the detection of high-resistivity body by transient electromagnetic method. In: *Proceedings 2011 International Conference on Transportation, Mechanical, and Utility Engineering (TMEE)*, 2011, pp. 1103-1106. <https://doi.org/10.1109/TMEE.2011.6199397>
- [13] Svatos J and Vedral J. The Usage of Frequency Swept Signals for Metal Detection. *IEEE Transactions on Magnetics* 2012, 48(4): 1501-1504. <https://doi.org/10.1109/TMAG.2011.2173174>
- [14] Tie CJ, Weng CC, Aydin AA., et al. Detection of buried targets using a new enhanced very early time electromagnetic (VETEM) prototype system. *IEEE Transactions on Geoscience and Remote Sensing* 2001; 39(12): 2702-2712. <https://doi.org/10.1109/36.975004>
- [15] Chang JH, Su BY, Malekian R, et al. Detection of Water-Filled Mining Goaf Using Mining Transient Electromagnetic Method. *IEEE Transactions on Industrial Informatics* 2019; 16(5): 2977-2984. <https://doi.org/10.1109/TII.2019.2901856>
- [16] Qi ZP, Li X, Li H, et al. First Results From Drone-Based Transient Electromagnetic Survey to Map and Detect Unexploded Ordnance. *IEEE Geoscience and Remote Sensing Letters* 2020; 17(12): 2055-2059. <https://doi.org/10.1109/LGRS.2019.2962754>
- [17] Su BY, Yu JC, Krczyk GM., et al. Innovative Surface-Borehole Transient Electromagnetic Method for Sensing the Coal Seam Roof Grouting Effect. *IEEE Transactions on Geoscience and Remote Sensing* 2022; 60: 5702509. <https://doi.org/10.1109/TGRS.2022.3149212>
- [18] Wang LJ, Zhang S, Chen SD, et al. Fast Localization of Underground Targets by Magnetic Gradient Tensor and Gaussian-Newton Algorithm With a Portable Transient Electromagnetic System. *IEEE Access* 2021; 9: 148469-148478. <https://doi.org/10.1109/ACCESS.2021.3124285>
- [19] Zhang JL, Xiang XB and Li WJ. Advances in Marine Intelligent Electromagnetic Detection System, Technology, and Applications: A Review. *IEEE Sensors Journal* 2023; 23(5): 4312-4326. <https://doi.org/10.1109/JSEN.2021.3129286>
- [20] Wang LJ, Zhang S and Chen SD. Underground Target Localization Based on Improved Magnetic Gradient Tensor With Towed Transient Electromagnetic Sensor Array. *IEEE Access* 2022; 10: 25025-25033. <https://doi.org/10.1109/ACCESS.2022.3156080>
- [21] Zhang XH, Pang XY, Yu SB, et al. A Broadband Multifrequency Resonance Compensator for Frequency-Domain Electromagnetic Prospecting Transmitting System. *IEEE Transactions on Power Electronics* 2024; 39(5): 5178-5193. <https://doi.org/10.1109/TPEL.2024.3358826>
- [22] Liu LH, Qiao L, Liu LS, et al. Applying Stray Inductance Model to Study Turn-off Current in Multi-Turn Loop of Shallow Transient Electromagnetic Systems. *IEEE Transactions on Power Electronics* 2020; 35(2): 1711-1720. <https://doi.org/10.1109/TPEL.2019.2923234>
- [23] Wu X, Xue GQ and He YM. The Progress of the Helicopter-Borne Transient Electromagnetic Method and Technology in China. *IEEE Access* 2020; 8: 32757-32766. <https://doi.org/10.1109/ACCESS.2020.2972916>
- [24] Oldenburg D W, Haber E and Shekhtman R. Three dimensional inversion of multisource time domain electromagnetic data. *Geophysics* 2013; 78(1): E47-E57. <https://doi.org/10.1190/geo2012-0131.1>
- [25] Jiang ZH, Liu LB, Liu SC, et al. Surface-to-Underground Transient Electromagnetic Detection of Water-Bearing Goaves. *IEEE Transactions on Geoscience and Remote Sensing* 2019; 58(8): 5303-5318. <https://doi.org/10.1109/TGRS.2019.2898904>
- [26] Xue GQ, Yu JC. New development of TEM research and application in coal mine exploration. *Progress in Geophysics* 2017; 32(1): 319-326. <https://doi.org/10.6038/pg20170145>